Dispersion-Dominated Photocurrent in Polymer:Fullerene Solar Cells

Armantas Melianas, Vytenis Pranculis, Andrius Devižis, Vidmantas Gulbinas, Olle Inganäs, and Martijn Kemerink**

Organic bulk heterojunction solar cells are often regarded as near-equilibrium devices, whose kinetics are set by well-defined charge carrier mobilities, and relaxation in the density of states is commonly ignored or included purely phenomenologically. Here, the motion of photocreated charges is studied experimentally with picosecond time resolution by a combination of time-resolved optical probing of electric field and photocurrent measurements, and the data are used to define parameters for kinetic Monte Carlo modelling. The results show that charge carrier motion in a prototypical polymer:fullerene solar cell under operational conditions is orders of magnitude faster than would be expected on the basis of corresponding near-equilibrium mobilities, and is extremely dispersive. There is no unique mobility. The distribution of extraction times of photocreated charges in operating organic solar cells can be experimentally determined from the charge collection transients measured under pulsed excitation. Finally, a remarkable distribution of the photocurrent over energy is found, in which the most relaxed charge carriers in fact counteract the net photocurrent.

1. Introduction

Carbon-based semiconductors allow for a low-cost alternative to inorganic solar cells. Extensive scientific and technological developments have recently led to organic solar cells with over 10% power conversion efficiency.[1,2] The majority of the investigated organic photovoltaic (OPV) cells are based on an intimate mixture of a conjugated polymer (donor) and a fullerene derivative (acceptor): a bulk heterojunction with intrinsic disorder, and thus localized electronic states. Functioning of these devices is understood as a sequence of steps; upon absorption of a photon by the donor (or acceptor) an exciton is created, which, via some charge transfer (CT) state is split into free charges that subsequently are transported to the appropriate electrodes after which they can deliver work in an external circuit. The last part of this chain of events constitutes a charge transport problem that sets the shape of the current-voltage characteristic of the operational device. The key parameters in this are the electron and hole mobilities: they set the time needed by the photocreated charges to be extracted from the device by the effective electric field, and determine how fast electrons and holes meet to recombine. It is common to make the implicit assumptions that these mobilities (a) correspond to the values in a near-equilibrium situation and (b) can be determined from many different kinds of experiments. Mobilities are thus considered a material constant (apart from a possible density or field dependence that are considered unimportant at the fields and densities encountered in OPV devices.[3–5] In fact, assumptions (a) and (b) convey a view on OPV cells as near-equilibrium devices that are at least in local thermal equilibrium so Fermi-Dirac statistics can be employed and local (quasi) Fermi levels can be defined. Empirically such a view seems fully justified by the success of drift-diffusion models in describing OPV current-voltage characteristics[4,6–9] and of Shockley-type models in describing the light intensity dependence of the open circuit voltage V_{OC}.[8,10–13] Here we demonstrate that these assumptions are invalid.

We combine transient electro-optical experiments and kinetic Monte Carlo modeling[14] on the representative, well-performing polymer:fullerene system TQ1:PCBM[15,16] to show that charge transport in OPV devices is orders of magnitude faster than that anticipated on basis of near-equilibrium mobilities. Moreover, the transport process is found to be extremely dispersive, leading to orders of magnitude spread in extraction times under operational conditions. The motion of photogenerated charges is highly diffusive and governed by relaxation in

A. Melianas, Prof. O. Inganäs
Department of Physics
Chemistry and Biology
Biomolecular and Organic Electronics
Center of Organic Electronics (COE)
Linköping University
58183, Linköping, Sweden
E-mail: armme@ifm.liu.se

V. Pranculis, Dr. A. Devižis, Prof. V. Gulbinas
Center for Physical Sciences and Technology, Savanorių 231
LT-02300 Vilnius, Lithuania

Prof. M. Kemerink
Department of Applied Physics
Eindhoven University of Technology
PO Box 513, 5600 MB Eindhoven, The Netherlands
E-mail: martijn.kemerink@liu.se

Prof. M. Kemerink
Department of Physics
Chemistry and Biology
Linköping University
58183, Linköping, Sweden

DOI: 10.1002/adfm.201400404

the disorder-broadened density of states (DOS). Consequently the mean carrier mobility is very much time dependent, in fact in an operational OPV device the majority of charges do not relax to (local) thermal equilibrium during their presence in the device. The incomplete relaxation gives rise to a remarkable energy dependence of the current density distribution, where in fact the most relaxed charge carriers move (diffusively) against the field, reducing the net photocurrent. Importantly, the dispersion in extraction times of photogenerated charges under CW operation at ~1 Sun can be experimentally determined from the response to pulsed (laser) illumination.

The transient motion of photocreated charges was probed over a wide range of times by combining time-of-flight, or time-resolved photocurrent measurements (TOF), with optical probing of the electric field by means of time-resolved electric field-induced second harmonic generation (TREFISH).[14,17] The time-resolution of conventional transient electrical measurements is limited to tens of ns. To measure photocurrents during the ps-ns time window we have therefore used an optical detection scheme enabling sub-picosecond time-resolution (see Experimental Section and SI section 6). The changing electric field due to the motion of photogenerated charge carriers is probed by recording the intensity of the EFISH signal, i.e. the second harmonic of the probe beam, which is electric field dependent as $\propto F^2$. The change in electric field can then be straightforwardly transformed into an amount of extracted charge (see SI section 6). Combining these techniques allows to follow the photocurrent response of our polymer:fullerene solar cell over six decades in time. While similar in methodology, the present work extends the previous work[14] by Vithanage et al. beyond the ns regime by combining TREFISH and TOF, and focuses on charge extraction dynamics rather than charge separation.

Having access to experimental information on charge motion down to the time scale of single hopping events is crucial for obtaining a complete physical picture of the operation of OPV devices. Kinetic Monte Carlo is the natural framework for interpreting ultrafast transport data as it offers a more direct, real space connection to the physical reality of charges hopping between localized states than for instance drift-diffusion models with time-dependent mobilities or a phenomenological tail of trap states. Even though transient phenomena like charge carrier relaxation and dispersion are inherently included in kinetic MC, they have so far received little attention, if any at all, as previous MC studies focused on steady-state phenomena and/or on mean values instead of on statistical spread. The unique time window offered by the combination of TREFISH and TOF experiments allows us to exploit the full potential of kinetic MC to follow processes in time.

2. Results

Figure 1a shows the amount of extracted charge with time, i.e. the integrated photocurrent measured under pulsed (550 nm) laser excitation. The indicated (reverse) bias is corrected for the built-in field of approximately –1 V. Given the low pump fluence used in this experiment (~ 5×10^{11} photons/cm^2 per pulse) we expect to be in the linear regime.

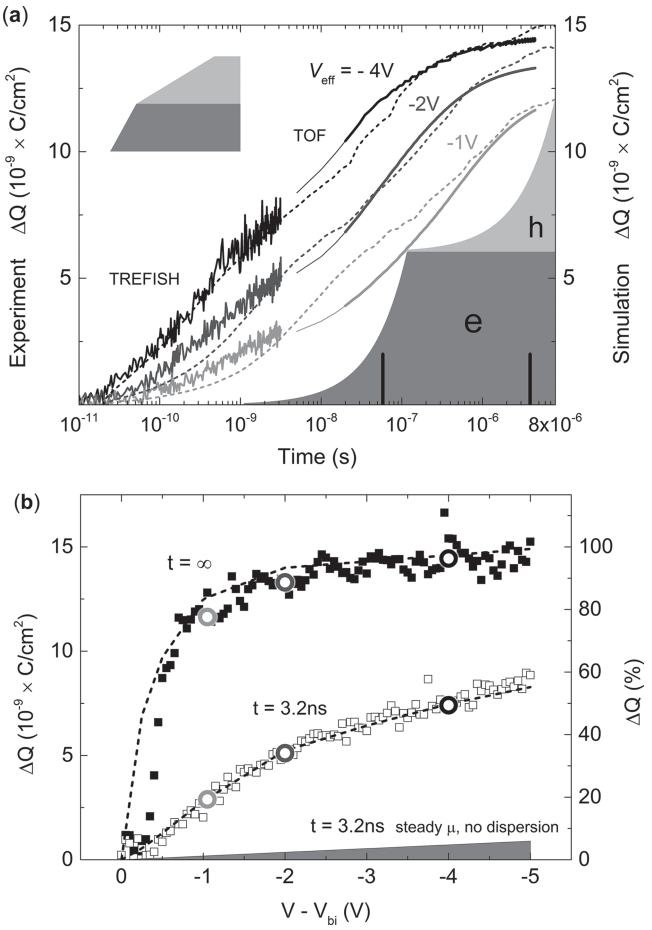

Figure 1. Charge extraction kinetics after pulsed excitation and its field dependence. (a) Combined TREFISH/TOF transients at different effective bias (solid lines) together with those obtained from Monte Carlo simulations (dashed lines). Due to limitations of electrical TOF measurements the initial ~20 ns might be unreliable and are marked by thinner lines. Shaded areas illustrate extraction in case of non-dispersive transport and steady-state mobilities; in this case mean extraction times for electrons and holes are ~0.06 μs and ~4 μs, respectively (black vertical bars). The inset schematically shows the same on a linear time scale. (b) Bias dependence of the amount of extracted charge after 3.2 ns (open squares) and of the total extracted charge (filled squares). The amount of extracted charge obtained in the time-resolved experiment in panel (a) (open circles) is in good agreement with the field dependence measurement and Monte Carlo simulations (dashed lines). The shaded area again indicates the estimated behavior for steady-state mobilities.

In order to interpret the experimental data in Figure 1a it is instructive to compare these to what would have been obtained in case charge transport was non-dispersive and governed by near-equilibrium mobilities. The hopping parameters used in the simulations (see SI section 2 for a detailed discussion) correspond to near-equilibrium mobilities of $\mu_e = 4 \times 10^{-4}$ cm^2/Vs and $\mu_h = 6 \times 10^{-6}$ cm^2/Vs, as calculated from Eq. (3) in Ref. [3] which we shall use here; comparison with experimentally determined mobilities shall be done below. Assuming a homogeneous generation profile, which is a reasonable approximation for the present semitransparent devices (see SI section 5), these mobilities translate into linear extraction profiles as schematically shown in the inset of Figure 1a. The linearity fol-

lows from the homogeneous electron and hole distributions being extracted at constant velocities. The first and the second step correspond to the electrons and holes being fully swept out of the device at an extraction time $t_{ex} = d^2/\mu_{e/h}V_{\text{eff}}$ with d the layer thickness and V_{eff} the effective voltage. For $V_{\text{eff}} = -1$ V, i.e. around short circuit, these traces are plotted as shaded areas in the main panel; the mobilities mentioned above give rise to mean electron and hole extraction times of 0.06 µs and 4 µs, respectively. On basis of the large difference in t_{ex} it may (in lowest order) be expected that the vast majority of electrons will have been extracted from the device before significant hole extraction takes place.

Two crucial features are evident when comparing the shaded area to the actual experiment. First, charge collection starts orders of magnitude faster than the near-equilibrium mobilities allow, i.e. they do not give a relevant estimate of the actual extraction time. Second, apart from underestimating how rapid extraction is also the shape of the extraction curve is completely different from that of the non-dispersive (linear) prediction; the experimental trace is close to log-linear. Since the horizontal axis may also be read as an extraction time this indicates that there is a wide distribution of extraction times. This can be attributed to dispersion or a time-dependent mean mobility. Below, we will show that both effects are important. In either case, the near-equilibrium mobility is a poor measure of the actual charge motion in operational solar cells; it not only underestimates the actual charge velocity by several orders of magnitude but also misses the wide spread in extraction times.

Deeper insight into the dispersive motion of photocreated charge carriers in OPV devices can be gained from the simulation of experimental data in Figure 1 by a kinetic Monte Carlo model, which is a well-established technique for this type of problem. The model accounts for the hopping charge motion in the energetically disordered donor-HOMO and acceptor-LUMO levels in the bulk heterojunction and keeps track of all Coulomb interactions as well as mono- and bimolecular recombination and diffusion; see the Experimental section and the Supporting Information for more details. Our Monte Carlo simulations (dashed lines in Figure 1) reproduce well the two key features of the experiment: the dispersive shape of the charge extraction curve and the fact that charge extraction is much faster than would be expected on basis of near-equilibrium mobilities.

The hopping parameters for the electrons and holes could be independently obtained from the bias-dependent TREFISH + TOF curves in Figure 1a by making use of the fact that electron extraction is almost complete before hole extraction commences. This method is not only justified on basis of the anticipated near-equilibrium mobilities but also by the exact shape of the TREFISH + TOF curves: they reveal intermediate saturation on a several ns time scale when approximately half of the total charge (electrons) is extracted. TREFISH experiments of a device with a thick active layer further support this claim, see additional TREFISH experiments (section 6 in SI). The part of the curve corresponding to the first half of extracted charges was therefore used to determine the electron hopping parameters; see SI, section 2, for an account of how the parameters have been estimated. Likewise the hole parameters have been obtained from the second half of extracted charges.

The field dependence of the amount of extracted charge is plotted in Figure 1b. It is indicated for the characteristic time of 3.2 ns, where the TREFISH measurement ends (open squares), and at long times when all charge is extracted (filled squares). At 3.2 ns significant hole extraction has not taken place, so only electron kinetics are probed. Clearly the simulation (dashed lines) captures the field dependence of the extraction kinetics very well. Apart from some deviations at low effective field, the total amount of extracted charge is well reproduced by the model, suggesting a reasonable description of recombination kinetics in this field regime. Recombination kinetics is, however, not the main purpose of the present work. The fact that equilibrium mobilities are a poor measure of the actual kinetics is once more highlighted by the shaded area, which has been calculated for steady-state mobilities while ignoring recombination and thereby forms an upper limit.

As discussed above, the large spread in extraction times of photocreated charges in OPV cells can either be due to dispersion or a time-dependent mean mobility or a combination of both. In contrast to the experiments, the MC calculations can easily separate the two effects. **Figure 2** (right y-axis) displays the transient mean total mobility, i.e. the sum of the mean electron and mean hole mobilities, extracted from Monte Carlo simulations with the same hopping parameters as used above. In line with the results in Figure 1 the mobility is far from constant; only beyond the µsec-range does it level off. The noise in the simulation at these times stems from the fact that by then the vast majority of charges have recombined, making it virtually impossible to reach converged results in this manner. Nevertheless the predicted steady-state total mobility, which is entirely dominated by the larger electron mobility, agrees quite well with the near equilibrium value for $\mu_e = 4 \times 10^{-4}$ cm^2/Vs and, more importantly, with the values obtained from the photo-CELIV (charge extraction by linearly increasing voltage) experiment (open circles).

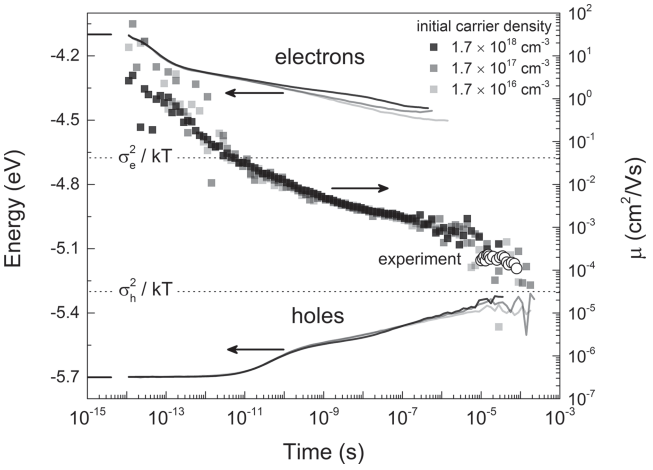

Figure 2. Simulated relaxation of photocreated charges and transient mobilities. Solid lines are electron and hole relaxation kinetics calculated for different initial carrier concentrations (grayscale) indicated in the legend. Relaxation starts at the HOMO –5.7 eV and LUMO –4.1 eV centers (black horizontal bars). Filled squares show the corresponding mean total mobility and the open circles show the transient mobility measured by photo-CELIV.

The simulation results in Figure 2 are essentially independent of the initial concentration, i.e. light intensity. That means that on the time and energy scales relevant to charge extraction in OPV devices carrier kinetics and relaxation are not significantly affected by state filling effects; this is in stark contrast to the corresponding near-equilibrium situation where state filling is important at much lower concentrations.[18] It thus allows to translate these results to OPV cells under steady state (CW, 1 Sun) operation.

3. Discussion

Let us now turn to the physical reason for the fast charge carrier motion and its dispersion. In earlier work, we have suggested their relevance to OPVs.[19,20] Also in a few recent papers the importance of fast, mainly diffusive motion of photogenerated charges was again highlighted.[14,21] This motion is driven both by entropic effects and by the ability of the charges to relax in the disordered density of states (DOS): white light excitation leads to electron and hole populations with mean energies at the center of the donor HOMO and donor LUMO (if significant exciton diffusion takes place this may cause some relaxation). However, as electron transfer to the acceptor is an energetically downward process this will, for statistical reasons, again lead to an electron population that is centered around the (acceptor) LUMO – assuming the electron is the charge that gets transferred; the hole population remains unchanged (and partially relaxed in case exciton diffusion is significant) upon charge transfer. Hence the electron and the hole can substantially relax in their respective DOS after charge transfer. This motion (a) is energetically downward even though the remaining CT binding energy of ~0.2 eV needs to be overcome[21,22] and (b) is therefore very fast. In contrast, near-equilibrium motion is governed by hops that are energetically upward (from the equilibrium energy to some transport energy)[23] and is therefore much slower.

The relaxation curves in Figure 2 (left y-axis) quantify the picture sketched above. Although exciton diffusion is incorporated in the MC simulations it does not lead to substantial relaxation before charge transfer takes place: it would give rise to simultaneous relaxation of the mean electron and hole energies which is not observed. Hence both the electron and the hole relax by hopping motion, starting at the acceptor LUMO energy (–4.1 eV) and the donor HOMO energy (–5.7 eV), respectively. Due to their faster hopping, electron relaxation starts before hole relaxation (see SI section 10). As relaxation continues, the number of 'easy' hops, i.e. energetically downward or only slightly up, decreases and therefore the mobility decreases. Note also that especially the electron population does not reach equilibrium (at an energy of $-\sigma^2/k_BT$ below the LUMO center): the line stops where poor statistics due to the vanishing population set in. The last remaining holes do reach near-complete relaxation which is due to the lesser disorder in the donor HOMO than in the acceptor LUMO (σ_h = 0.1 eV vs. σ_e = 0.12 eV) which greatly affects the relaxation speed.[24] This does not mean that *all* holes have relaxed before leaving the device, as will be extensively discussed in the sections below.

The main topic of this paper is dispersive charge dynamics. We shall, however, in this paragraph briefly address the relation of the present findings with earlier works focusing on charge separation in similar systems. The simulations as presented above predict an exciton-to-free charge dissociation yield of 0.89 at short circuit, which is fully consistent with the measured IQE of ~0.90. This dissociation probability only drops when a CT complex is formed in which initially both the electron and the hole sit on low-lying sites, i.e. sit substantially below the DOS center.[21] This is consistent with a recent experimental work in which it was shown that IQEs of 90% and above can be maintained for long-wavelength excitation: no difference between excitation in the center of the CT band and in the donor S1 state was found.[25] The efficient free charge generation is an emergent property of our kinetic MC treatment in combination with the parameters used. The present results are, however, consistent with the mechanism for charge separation put forward in Ref. [21] and in fact extend those results to operational OPV devices and state-of-the-art materials. In Ref. [21] it was argued that the energy loss associated with relaxation of photocreated charges in a disordered DOS is of the same order or larger than the binding energy of a CT complex and can therefore be used to efficiently dissociate a CT complex into free charges (see SI section 3 for an illustrative cartoon). Figure 2 shows that also for the TQ1:$PC_{71}BM$ system the energy loss by electron relaxation is substantially larger than the CT binding energy of around 0.2 eV.[22] In addition, entropic effects, that are automatically included in the MC simulations, further enhance separation efficiency.[14,26] We conclude this paragraph by noting that although the P3HT:PCBM system in Ref. [14] and our TQ1:PCBM system give rather similar responses in TREFISH, corroborating the general nature of the present conclusions, Ref. [14] focusses entirely on the implications for charge separation, not addressing dispersion.

The energies and mobilities discussed so far are statistical means for the populations surviving at the indicated time. Hence, variations *within* these populations are not shown. In fact, such variations are an important cause for dispersion. As hopping charge motion is a statistical process, charges that happen to hop to a (very) low-lying state will take (very) long to be extracted. Conceptually it is tempting to consider such deep states as traps;[27] however, there is no fundamental difference between deeper and less deep states in the (Gaussian) DOS. In all cases charge motion, and concomitant relaxation is by hopping between localized states in a disordered energy landscape.

The dispersive motion of photocreated electrons and holes is characterized in **Figure 3**. The top panel of Figure 3a shows the transient mean electron and hole mobilities calculated for the TREFISH/TOF experiment in Figure 1a at $V_{eff} = -1$ V (see SI section 8 for dispersion at MPP). As expected, at long times both relax to the steady-state values indicated by the horizontal bars. These confirm that the measured photo-CELIV mobilities (filled and open symbols) reflect a near-equilibrium value for electrons and holes. The middle panel shows the distribution functions (per unit log-time) of the electron and hole extraction times (dark grey and light grey shaded areas, respectively), i.e. the time needed for each charge to be extracted after its photocreation. As these histograms have an approximately log-normal shape, their means sit on the right

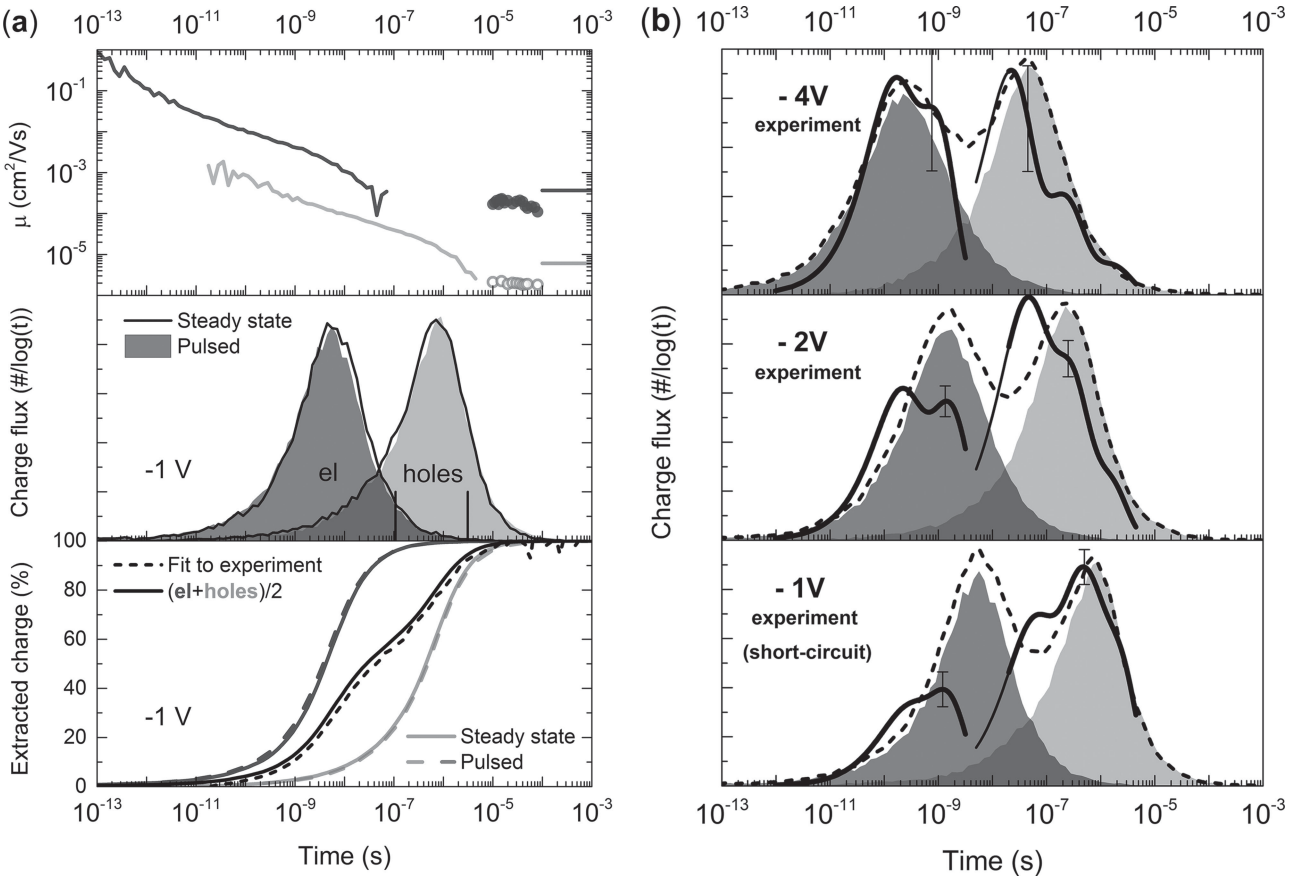

Figure 3. Dispersion in mobility and charge extraction time. (a) Top panel: simulated charge carrier mobility relaxation with time for electrons (dark grey) and holes (light grey) during a combined TREFISH/TOF experiment at $V_{eff} = -1$ V. Horizontal bars are corresponding steady-state mobilities, symbols show photo-CELIV mobilities for the TQ1:$PC_{71}BM$ device (filled dark grey circles) and for a TQ1 film (open light grey circles). Middle panel: extraction time distribution functions for the TREFISH/TOF data simulations (shaded areas); identical results are obtained for steady-state device simulations at short circuit and ≈1 Sun (solid lines). Vertical bars indicate mean extraction times. Bottom panel: comparison of an explicit TREFISH/TOF simulation ($V_{eff} = -1$ V, dashed black line) with the average (solid black line) of the integrated electron and hole extraction time distributions under steady state (solid dark grey and light grey lines respectively); Solid (steady-state simulation) and dashed (TREFISH/TOF simulation) lines are the log-integrals of the distributions presented in the middle panel, showing the fraction of total extracted charge. (b) Experimental charge carrier extraction time distributions (thick solid lines) obtained as the log-time derivate of the (smoothed) experimental data in Figure 1a; The time interval 5–20 ns might be unreliable and is marked by thin solid lines as in Figure 1a. Dashed lines are the same procedure applied to the simulation curves. Shaded areas are the corresponding simulated extraction time distributions.

hand side of the mode (maximum) as indicated by the vertical bars.

The normalized integrals of the distribution functions are presented in the bottom panel and reflect the fraction of charges that have been extracted after a certain time. Importantly, at the mean extraction time, about 80–90% of all photocreated charges have been extracted already. In fact, about 50% of all charges are more than an order of magnitude faster than the mean. This shows, once more, that mean extraction times are a very poor measure of the actual kinetics in OPV devices.

A crucial question is whether the TREFISH/TOF results, obtained after pulsed excitation, can be directly translated to operational solar cells that are CW excited with lower light intensity and concomitant lower charge densities. The affirmative answer to this question lies in the comparison of the above discussed results with simulations carried out with exactly the same parameters and (homogeneous) generation profile as in the TREFISH/TOF simulations but using continuous excitation with approximately 1 Sun intensity. The solid black lines in Figure 3a (middle panel) show the extraction time distribution functions obtained from device simulations under steady state, which now reflect the time lag between carrier photogeneration and extraction. Good agreement between distribution functions is obtained from simulations under pulsed and CW (steady state) illumination conditions. This shows that pulsed excitation adequately reflects processes under CW excitation. Consequently, the averaged sum of the integrated electron and hole distributions as obtained from simulation under CW excitation perfectly reproduces carrier extraction kinetics obtained from simulations under pulsed excitation (solid black and dashed black lines in bottom panel of Figure 3a). This is a key result as it allows to make statements about the dispersive charge kinetics during normal (CW, ~1 Sun) solar cell

operation on basis of pulsed (laser) measurements, as will be discussed below.

The bottom panel of Figure 3a shows that, at least for sufficiently thin devices, the shape of the TREFISH/TOF response curve (dashed black line) is equal to the sum of the integrated distribution functions during steady-state operation (solid black line). The important consequence is that by calculating the log-time derivative of the TREFISH/TOF curve the distribution of extraction times in the solar cell under CW (1 Sun) operation can be obtained. This is shown in the b panel of Figure 3 where the thick solid lines are now the experimental extraction time distribution functions obtained as $d(\Delta Q)/d(\log t)$ of the (smoothed) experimental data in Figure 1(a). Smoothing was accomplished by separately fitting TREFISH and TOF data by a sum of exponentials and is the cause of the small additional bumps in the experimental curves. Fitting converged at 2 and 3 exponentials for the TREFISH and TOF respectively. Error bars indicate the largest error if a different number of exponentials (3 and 2 respectively) would have been used instead. The dashed curves show the distributions obtained by applying the same method to the corresponding MC simulations. Given the noise in the experiments the agreement between distributions obtained from experimental and simulated data is rather satisfactory: a double peak structure is clearly visible, confirming the previously assumed time lag between electron and hole extraction. Moreover, the simulations do follow the experiments both in the magnitude of the dispersion, as can be measured by the shape and width of the separate peaks, and in the position and field dependence of the peak maxima.

The strong dispersion in extraction times shown in Figure 3 suggests that in operational solar cells most of the photocurrent is carried by the fastest charges, i.e. the charges that do not get stuck in a deep site. On the other hand charges that make up most of the density of occupied states (DOOS) are those that do get stuck and cause a build-up of space charge. The left panel of **Figure 4**a shows that this intuitive distinction between more and less mobile charges can indeed be made. Plotted are the simulated steady-state electron and hole DOOS obtained from device simulations during CW ≈ 1 Sun illumination at $V_{\text{eff}} = -0.2$ V (≈maximum power point (MPP), solid lines) and at $V_{\text{eff}} = -1.0$ V (short-circuit, dashed lines). Due to the higher electron mobility the electron DOOS is lower than the hole DOOS; both decrease with increasing field as expected. Note that the DOOS peaks do not lay at σ^2/k_BT (dotted lines) below the LUMO or above the HOMO center, indicating incomplete thermalization of charge carrier distributions under steady-state conditions. This reflects the fact that charges typically leave the device, either by extraction or recombination, before they have thermalized in the DOS. In this context it is crucial to keep in mind the difference between thermalization by hopping around in an energetically disordered landscape, which is considered here, and on-site thermalization (not considered) in, for instance, a vibrational manifold.[26]

More surprising is the energy-resolved current density in the right panel of Figure 4(a); $j(E)$ is a distribution function of the current density over energy; integrating $j(E)$ gives the total current density that is positive and equal for both electrons and holes. Both the electrons and the holes show a positive

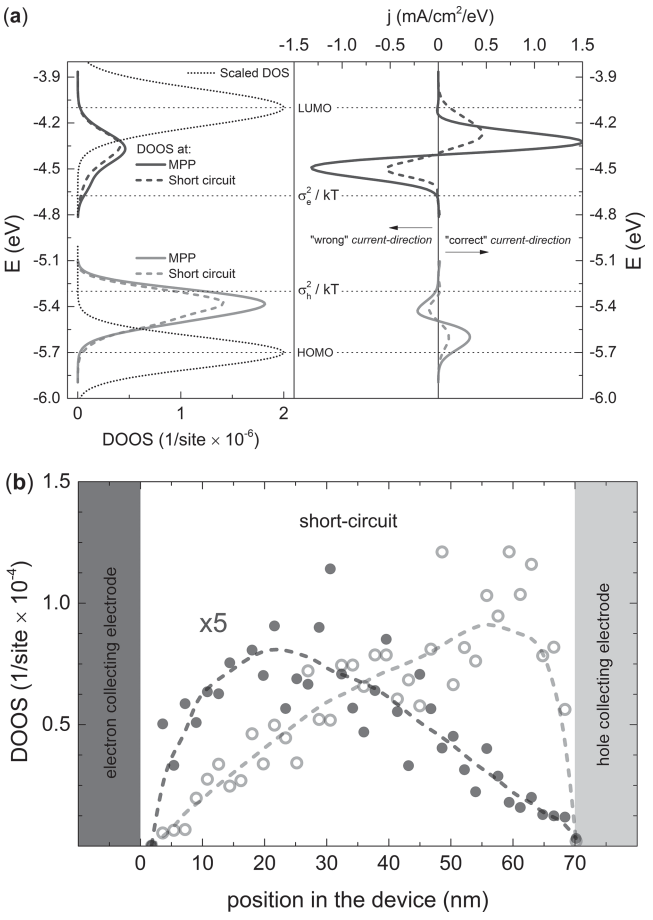

Figure 4. Energy distribution of charge and current density. (a) Left panel: DOOS distributions of electrons (dark grey) and holes (light grey) simulated during steady-state operation at ~1 Sun for MPP (–0.2 V) and short circuit (–1 V). HOMO and LUMO DOS are indicated as dotted lines (not to scale). Right panel: corresponding energy-resolved current density (top x-axis) showing the contributions to photocurrent from charge carriers at different energies. (b) Corresponding charge density profiles at short-circuit for electrons (filled circles) and holes (open circles). Dashed lines are a guide to the eye.

contribution to the total current from lesser relaxed carriers and a smaller, negative contribution from more relaxed carriers. The positive and negative current peaks are due to, respectively, the drift and the net diffusion contributions to the total current. The drift contribution simply follows the direction of the electric field and is therefore positive. The negative sign of the net diffusion contribution can be understood as follows: taking the holes as an example, the hole current density increases towards the hole extracting contact which follows from the fact that charges generated in an increasingly large fraction of the total film thickness contribute to the (local) current density.[28] From this and the fact that charges that traveled longer distances will be further relaxed it follows that also the hole density increases towards the hole extracting contact as shown in Figure 4(b). This leads to a charge density gradient (a) that is mostly directed away from the extracting contact and (b) that consists mainly of 'relaxed' holes. Hence the sign of the net diffusion current is negative and the peak in the hole DOOS

coincides with the negative peak in $j(E)$. Similarly the same can be explained for electrons. Hence, further relaxed charges do not only contribute less to the net current, they in fact counteract the net current due to the negative density gradient that gives rise to diffusion away from the contact. It should be kept in mind that drift and diffusion currents running in opposite directions are a well-understood characteristic of Ohmic contacts in general.[29] The distinct feature of the situation in Figure 4 is that these currents flow at different energies, once more highlighting that the system is far from equilibrium.

A practical implication of the above results is that mobilities found in one experiment are not necessarily relevant to the other, even if both are in the same density regime. The strong time dependence of the mobility of photocreated charges in combination with the fact that the vast majority of these charges get extracted before full thermalization occurs makes mobilities from 'slow' experiments, that effectively probe the mobility of (almost) completely relaxed charges, like space charge limited currents (SCLC) (see SI section 4 for an example) and photo-CELIV of limited relevance for understanding operational OPV. Mobilities extracted from dark current-voltage characteristics of OPV devices are therefore not particularly suited to make statements about the kinetics underlying the corresponding light current-voltage curve. Likewise, expressing recombination rates in operational OPV in terms of equilibrium mobilities seems of limited use. Even the relevance of properly defined and measured time-dependent mean mobilities is limited in view of the strong dispersion in extraction times.

4. Conclusion

We have studied the ultrafast charge transport of photocreated charges in a typical organic bulk heterojunction photovoltaic device. Charge extraction is experimentally shown to be highly dispersive, with which it is meant that (a) the mobility depends very strongly on time after photo-creation and that (b) there is a large spread in charge extraction times, covering multiple orders of magnitude. Using the experimental data to define parameters for kinetic Monte Carlo modelling, the dispersion is shown to be due to relaxation of photo-generated charges in the disordered density of states; on the length scale of the device thickness charge motion is completely dominated by this relaxation. In fact, due to the (deliberate) simplicity of the Monte Carlo model, which excludes potential additional sources of dispersion in blends due to e.g. non-perfect percolation of PCBM (and polymer) domains creating spatial rather than energetical traps, the calculated dispersions should, for the used parameters, be considered as a lower limit. In either case, there is no unique mobility in an operational OPV device. We have, however, shown that the extraction time distribution of photo-generated charges, which is a relevant measure of the dispersion of an OPV device under operational conditions, can be determined from measured pulse responses. Moreover, we demonstrated that charge kinetics are orders of magnitude faster than what would be expected on basis of near-equilibrium mobilities. Finally, the out-of-equilibrium charge carrier distributions give rise to a remarkable distribution of the photocurrent over energy, with the most relaxed charges in fact diffusing against the electric field, reducing the net photocurrent. Care should therefore be taken when employing formalisms that implicitly or explicitly assume a near-equilibrium situation to be present in operating OPV cells.

5. Experimental Section

Materials: We have studied polymer:fullerene solar cells based on a bulk heterojunction of poly[2,3-bis-(3-octyloxyphenyl)quinoxaline-5,8-diyl-*alt*-thiophene-2,5-diyl] (TQ1):[6,6]-phenyl-C71-butyric acid methyl ester ($PC_{71}BM$).[15] TQ1 is a liquid crystalline polymer, with an internal donor-acceptor motif of thiophene and quinoxaline.[15] When mixed with $PC_{71}BM$ the later shows small degrees of crystallization.[30] As such, TQ1:$PC_{71}BM$ is an archetypical system and the results that follow are expected to apply to a broad range of disordered polymers.

Sample Fabrication: Semitransparent solar cells in inverted geometry with the following structure: ITO/PFPA-1/TQ1:$PC_{71}BM$/PEDOT:PSS (Clevios PH1000) were investigated (See SI section 1 for device characteristics). The used donor-acceptor ratio is 1:2.5. The active layer thickness was 70 nm as measured with a Dektak surface profilometer. Detailed information on sample fabrication, device parameters etc. can be found in Ref.[31] The thick active layer (440 nm) solar cell was fabricated in the same manner, except that the active layer was drop-casted from an ODCB solution and allowed to dry in the glove box. The neat TQ1 film for photo-CELIV measurements was blade-coated from an ODCB solution. Electron-only devices were fabricated in the following geometry: Al/TiO_x/TQ1:$PC_{71}BM$/LiF/Al, hole-only devices: ITO/PEDOT:PSS/TQ1:$PC_{71}BM$/PEDOT:PSS (PH1000). Active layers were spin-coated using identical settings as for the solar cell device.

TREFISH and Integral Mode Time-of-Flight (TOF) Measurements: These were performed simultaneously, i.e. measuring the response of the solar cell from the same pump pulse. For integral mode TOF measurements a 10 kΩ load was used. Matching to TREFISH is achieved by shifting all TOF traces by –20 ns due to the uncertainty of $t = 0$. The absolute height is corrected by an experimentally determined scaling factor, which accounts for the nonhomogeneous illumination of the entire sample area. Samples were pumped through the PEDOT side with a 550 nm laser at 980 Hz repeat rate and a pump fluence of 5×10^{11} photons/cm^2 per pulse. Probing was through the PEDOT side at a wavelength of 800nm and a fluence of 2.8×10^{15} photons/cm^2 per pulse. However, absorbance of the sample was negligible at the probe wavelength, thus sample exciation by the probe was insignificant. The probe detector was placed on the ITO side. The temporal resolution of this experiment is limited only by the duration of the laser pulses used (≈120 fs), allowing for sub-ps time resolution. The working principle of TREFISH is described in detail elsewhere.[17] Briefly, the changing electric field due to the motion of photogenerated charge carriers is probed by recording the intensity of the EFISH signal, i.e. the second harmonic of the probe beam, which is electric field dependent as $\propto F^2$ (see SI section 6). The change in electric field can then be straightforwardly transformed into an amount of extracted charge $Q(t) = CdF(t)$ with d the layer thickness. This implies that the field distribution within the sample thickness has to be homogeneous (see SI sections 5 and 6). This is mostly assured by measuring at pump fluencies which do not induce field changes larger than 10% of the applied field. As exciton dissociation occurs on much shorter timescales than investigated here, the excitonic contribution to the TREFISH signal is not observed and thus ignored.[17]

Photo-CELIV Experiments: These were performed on TQ1:$PC_{71}BM$ devices and pure TQ1 films. Charge carriers are photogenerated by a ns laser pulse (500 nm) and after a variable time delay extracted by a linearly increasing voltage (CELIV). From the temporal position of the extraction current maximum charge carrier mobility can be estimated. The formula used for calculation depends on the approximation method employed. In this work it was estimated as suggested by Juška.[32]

Kinetic Monte Carlo Model: This accounts for the hopping charge motion in the energetically (Gaussian) disordered HOMO and LUMO levels of the donor and acceptor materials, respectively. Exciton diffusion

via the Förster and Dexter mechanisms is accounted for. Infinite slabs of material are simulated using periodic boundary conditions in the *x*,*y*-directions. Metallic contacts sit on either side of this slab. The full Coulomb interaction between all charges and their image charges that arise due to the metal contacts and the periodic boundary conditions are accounted for. Simulations in Figure 2 were carried out with periodic boundary conditions in all directions (i.e. no contacts) in the presence of a small electric field to enable determining the mobility without affecting it (1 V/100 nm). Charges sitting on the same site or on a nearest neighbor site are, respectively, treated as excitons and charge transfer (CT) complexes that can recombine with certain (different) rates. A detailed description of the model is given in the SI, section 2, where also the used parameter values are listed and motivated.

Supporting Information

Supporting Information is available from the Wiley Online Library or from the author.

Acknowledgements

We gratefully acknowledge contributions and discussions from Mingtao Lu, Zheng Tang, Wolfgang Tress, Tom J. Savenije, Jonas Bergqvist and D.H.K. Murthy. TQ1 was synthesized by Ergang Wang and Mats Andersson at Chalmers University of Technology. Research on organic photovoltaics in Linköping University is supported by the Swedish Science Council (VR) and the Swedish Energy Agency, and the Knut and Alice Wallenberg foundation through a Wallenberg Scholar grant to Olle Inganäs. Research in Vilnius CPST was partly funded by the European Social Fund under the Global Grant measure.

Received: February 6, 2014
Revised: February 28, 2014
Published online: April 22, 2014

[1] J. You, L. Dou, K. Yoshimura, T. Kato, K. Ohya, T. Moriarty, K. Emery, C.-C. Chen, J. Gao, G. Li, Y. Yang, *Nat. Commun.* **2013**, *4*, 1446.
[2] M. A. Green, K. Emery, Y. Hishikawa, W. Warta, E. D. Dunlop, *Prog. Photovolt. Res. Appl.* **2013**, *21*, 827.
[3] W. F. Pasveer, J. Cottaar, C. Tanase, R. Coehoorn, P. A. Bobbert, P. W. M. Blom, D. M. de Leeuw, M. A. J. Michels, *Phys. Rev. Lett.* **2005**, *94*, 206601.
[4] L. J. A. Koster, E. C. P. Smits, V. D. Mihailetchi, P. W. M. Blom, *Phys. Rev. B* **2005**, *72*, 085205.
[5] T. G. J. van der Hofstad, D. Di Nuzzo, S. van Reenen, R. A. J. Janssen, M. Kemerink, S. C. J. Meskers, *J. Phys. Chem. C* **2013**, *117*, 3210.
[6] K. Maturová, S. S. van Bavel, M. M. Wienk, R. A. J. Janssen, M. Kemerink, *Nano Lett.* **2009**, *9*, 3032.
[7] T. Kirchartz, J. Nelson, *TWWopics in Current Chemistry,* Springer-Verlag, Berlin/Heidelberg **2013**, pp.1–46.
[8] J. C. Blakesley, D. Neher, *Phys. Rev. B* **2011**, *84*, 075210.
[9] W. Tress, K. Leo, M. Riede, *Phys. Rev. B* **2012**, *85*, 155201.
[10] L. J. A. Koster, V. D. Mihailetchi, R. Ramaker, P. W. M. Blom, *Appl. Phys. Lett.* **2005**, *86*, 123509.
[11] A. Maurano, R. Hamilton, C. G. Shuttle, A. M. Ballantyne, J. Nelson, B. O'Regan, W. Zhang, I. McCulloch, H. Azimi, M. Morana, C. J. Brabec, J. R. Durrant, *Adv. Mater.* **2010**, *22*, 4987.
[12] K. Vandewal, K. Tvingstedt, A. Gadisa, O. Inganäs, J. V. Manca, *Nat. Mater.* **2009**, *8*, 904.
[13] N. C. Giebink, G. P. Wiederrecht, M. R. Wasielewski, S. R. Forrest, *Phys. Rev. B* **2010**, *82*, 155305.
[14] D. A. Vithanage, A. Devižis, V. Abramavičius, Y. Infahsaeng, D. Abramavičius, R. C. I. MacKenzie, P. E. Keivanidis, A. Yartsev, D. Hertel, J. Nelson, V. Sundström, V. Gulbinas, *Nat. Commun.* **2013**, *4*, 2334.
[15] E. Wang, L. Hou, Z. Wang, S. Hellström, F. Zhang, O. Inganäs, M. R. Andersson, *Adv. Mater.* **2010**, *22*, 5240.
[16] Y. Kim, H. R. Yeom, J. Y. Kim, C. Yang, *Energy Environ. Sci.* **2013**, *6*, 1909.
[17] A. Devižis, A. Serbenta, K. Meerholz, D. Hertel, V. Gulbinas, *Phys. Rev. Lett.* **2009**, *103*, 027404.
[18] R. Coehoorn, W. F. Pasveer, P. A. Bobbert, M. A. J. Michels, *Phys. Rev. B* **2005**, *72*, 155206.
[19] L. Mattias Andersson, O. Inganäs, *Chem. Phys.* **2009**, *357*, 120.
[20] L. M. Andersson, A. Melianas, Y. Infahasaeng, Z. Tang, A. Yartsev, O. Inganäs, V. Sundström, *J. Phys. Chem. Lett.* **2013**, *4*, 2069.
[21] H. van Eersel, R. A. J. Janssen, M. Kemerink, *Adv. Funct. Mater.* **2012**, *22*, 2700.
[22] J. Kern, S. Schwab, C. Deibel, V. Dyakonov, *Phys. Status Solidi RRL – Rapid Res. Lett.* **2011**, *5*, 364.
[23] J. Cottaar, L. J. A. Koster, R. Coehoorn, P. A. Bobbert, *Phys. Rev. Lett.* **2011**, *107*, 136601.
[24] W. C. Germs, J. J. M. van der Holst, S. L. M. van Mensfoort, P. A. Bobbert, R. Coehoorn, *Phys. Rev. B* **2011**, *84*, 165210.
[25] K. Vandewal, S. Albrecht, E. T. Hoke, K. R. Graham, J. Widmer, J. D. Douglas, M. Schubert, W. R. Mateker, J. T. Bloking, G. F. Burkhard, A. Sellinger, J. M. J. Fréchet, A. Amassian, M. K. Riede, M. D. McGehee, D. Neher, A. Salleo, *Nat. Mater.* **2013**, *13*, 63.
[26] T. M. Clarke, J. R. Durrant, *Chem. Rev.* **2010**, *110*, 6736.
[27] N. Christ, S. W. Kettlitz, S. Züfle, S. Valouch, U. Lemmer, *Phys. Rev. B* **2011**, *83*, 195211.
[28] For a film of thickness L with the electron and hole extracting contacts at z = 0 and z = L, respectively, the total current density is proportional to j_{tot}~qGL with G the generation rate. Considering a plane at a depth z, the electron current density through that plane is j_e ~ qG(L-z) and for the hole current j_h ~ qGz so that their sum equals j_{tot} everywhere, fulfilling current conservation. So both j_e and j_h increase towards their respective extracting contacts.
[29] M. Kemerink, J. M. Kramer, H. H. P. Gommans, R. a. J. Janssen, *Appl. Phys. Lett.* **2006**, *88*, 192108.
[30] E. Wang, J. Bergqvist, K. Vandewal, Z. Ma, L. Hou, A. Lundin, S. Himmelberger, A. Salleo, C. Müller, O. Inganäs, F. Zhang, M. R. Andersson, *Adv. Energy Mater.* **2013**, *3*, 806.
[31] Z. Tang, Z. George, Z. Ma, J. Bergqvist, K. Tvingstedt, K. Vandewal, E. Wang, L. M. Andersson, M. R. Andersson, F. Zhang, O. Inganäs, *Adv. Energy Mater.* **2012**, *2*, 1467.
[32] A. J. Mozer, G. Dennler, N. S. Sariciftci, M. Westerling, A. Pivrikas, R. Österbacka, G. Juška, *Phys. Rev. B* **2005**, *72*, 035217.